SUPPORTING INFORMATION

DYNAMICS OF RS-(AU-SR)$_x$ STAPLE MOTIFS ON METAL SURFACES: FROM NANOCLUSTERS TO 2D SURFACES

Pilar Carro[1], Evangelina Pensa[2,†,*], Tim Albrecht[2,$], Roberto C. Salvarezza[3]

[1]Área de Química Física, Departamento de Química, Facultad de Ciencias, Universidad de La Laguna, Instituto de Materiales y Nanotecnología, Avda. Francisco Sánchez, s/n 38200-La Laguna, Tenerife, Spain

[2]Imperial College London, Department of Chemistry, Exhibition, Road, London SW7 2AZ, UK

[3]Instituto de Investigaciones Fisicoquímicas Teóricas y Aplicadas (INIFTA), Facultad de Ciencias Exactas, Universidad Nacional de La Plata, CONICET, La Plata 1900, Argentina

CONTENTS

FIGURES

TABLES

*CORRESPONDING AUTHOR: e.pensa@tum.de

PRESENT ADDRESS: †Physics of Synthetic Biological Systems-E14, Physics-Department and ZNN, Technische Universität München, 85748, Garching, Germany

$School of Chemistry, University of Birmingham, Edgbaston Campus, Birmingham B15 2TT, United Kingdom

Scanning Tunneling Microscopy (STM).

Table S1. STM imaging conditions.

System	Figure	SetPoint tunnelling current [nA]	E_{bias} [V]	Scan rate [lines·s^{-1}]	Resolution [lines x lines]
$Au_{25}(SR)_{18}$ on Au(111) in Air	1a	0.30	0.20	4.039	1024x1024
	1c	0.70	0.50	12.12	1024x1024
	1d	0.70	0.50	12.12	1024x1024
	2a	0.60	0.70	12.12	1024x1024
	S3	0.60	0.70	12.12	1024x1024
$Au_{25}(SR)_{18}$ on Au(111) in mesitylene	2b-c	1.00	0.10	12.12	1024x1024
	2d-f	1.00	0.10	12.12	1024x1024
	4a-b	1.00	0.10	12.12	1024x1024
Au(111) in air	S1a	0.50	0.50	6.059	1024x1024
Au(111) in mesitylene	S1b	0.30	0.20	12.12	1024x1024

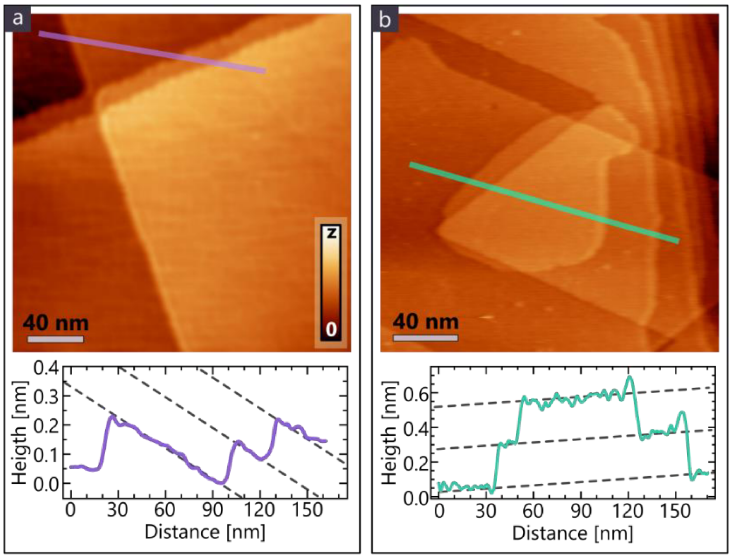

Figure S1. STM images of Au(111) before immersion in AuNC dispersions. Images were acquired in (a) in air and (b) mesitylene. The lower panels show the cross sections corresponding to the solid lines on each image. Dotted lines are included to highlight that the distance between Au steps agree with the one between monoatomic layers of Au(111) -i. e. 0.24 nm. For both images, the height-colour palette is the one shown in image (a) with a z value of 0.8 nm for (a) and 1.2 nm for (b).

Experimental determination of Au island coverage (θ_{Au})

The Au island coverage was determined as the area covered by the Au islands. For the analysis, we only take into account images where Au islands are on the top large terraces and far apart to the step edges. The "flooding" tool in WSxM software[3] was employed. As shown Figure S3, the height-threshold was adjusted in order to only account the Au islands and remove the rest of the surface (blue background in figure S3b). Then, the tool automatically calculates the area of the remaining islands relative to the total area of the image, which is indeed the coverage of Au islands (θ_{Au}).

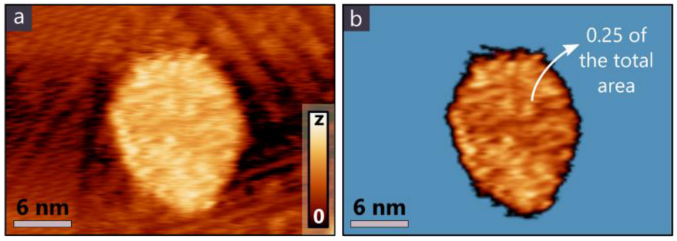

Figure S2. Determination of the area covered by Au islands. The "flooding" tool included in the WSxM software was employed. (a) Original image. (b) Flooded image. For the height-colour palette in (a) the z value is 0.6 nm.

Experimental determination of the thiolate reduction charge

The thiolate reduction charge, $q_{RS,}$ was determined according to

$$q_{RS} = B \frac{A_{SR}}{v_{SR}} \frac{v_{Au}}{A_{Au}} \qquad [S1]$$

where A_{SR} is the area of the thiolate electroreduction peak (shadowed area in Figure S3a), A_{Au} is the peak area of the electroreduction of Au oxide layer (shadowed area in Figure S3b), v_{SR} and v_{Au} are the scan rates at which the CVs were recorded and, B is a proportional constant that accounts for the charge provided for the oxidation of 1 cm^2 of Au(111) surface i.e. B= 444µC cm^{-2}.[4]

In order to determine the areas A_{RS} and A_{Au} the following protocol was applied. First, the electroreduction of thiolate-Au bond was performed. The potential was scanned in the cathodic direction at 0.1 V s^{-1} between -0.2 to -1.3 V to then back in the anodic direction to -0.2 V at the same scan rate. The resulting cyclic voltammogram (CV) is shown in Figure S3a (blue curve). During the cathodic scan, a sharp peak is observed at -0.97 ± 0.02 V as a result of the electroreduction of thiolate-Au bonds accordingly to RS-Au + e- → RS^- + Au^0 (RS: thiol molecule).[5] A_{RS} is then determined by integration as shown shadowed blue area in Figure S3a.

Immediately after the electroreduction of the thiols, the potential was cycled between to -1.35 V and 0.6 V at 0.1 V s^{-1}, until no signal associated with Au-thiol reduction was observed (ca. 20 cycles) and the Au voltammogram remained unchanged. The voltammogram of bare Au is shown in Figure S2b. During the anodic scan a monolayer of Au oxide is generated, giving the peaks at 0.05 and 0.35V. In the reverse scan, the whole layer is reduced in a single peak at ca. 0.05 V. Therefore, A_{Au} is obtained by integration of the reduction peak, as shown yellow-colored area in Figure S3b.

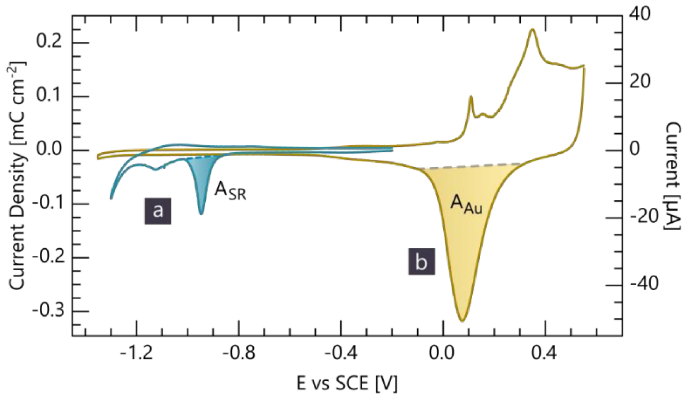

Figure S3. Thiolate surface coverage obtained by cyclic voltammetry. Voltammograms of Au(111) after immersion in 2 µM DCM dispersion of $Au_{25}(SR)_{18}$. CVs were recorded in NaOH 0.1 M at 0.1 V s^{-1}. Shadowed areas correspond to the integrated area employed in equation S1.

Derivation of the expression for the expected Au island coverage $\theta_{Au_{island}}$ for the different decomposition mechanisms of the AuNC' capping layer

By decomposition of a single AuNC, an amount of n_{RS} hexanothiolates and n_{Au} of Au atoms (that forms the Au islands observed by STM) are adsorbed on the substrate. As discussed in the main manuscript, due to the stoichiometry of the AuNC, n_{RS} is equal to 18, independently of the decomposition mechanism. On the contrary, n_{Au} does depend on the degree of decomposition of the capping layer (RS-Au-(RS)-Au-RS), as shown in table S2.

The RS and Au island coverages can be expressed through the AuNC surface density, n_{AuNC} as:

$$\theta_{RS} = n_{AuNC}\, n_{RS} \qquad [S2]$$

$$\theta_{Au_{island}} = n_{AuNC}\, n_{Au} \qquad [S3]$$

q_{RS} can be obtained from electrochemistry data allowing the calculation of the RS coverage, θ_{RS}, by means of the Au(111) unit cell area, $A_{Au(111)}$ and the elemental charge, *e*,

$$\theta_{RS} = \frac{q_{RS}}{e} A_{Au(111)} \qquad [S4]$$

The θ_{RS} data allows to deduce the surface density of AuNC from equation S2, $n_{AuNC} = \theta_{RS}/18$. Substituting this expression into equation S3, the Au island coverage can finally be estimated:

$$\theta_{Au_{island}} = \frac{\theta_{RS}\, n_{Au}}{18} \qquad [S5]$$

Hence, the expected Au island coverage $\theta_{Au_{island}}$ can be obtained by using equation S5 where n_{Au} values depend on the AuNC decomposition mechanism. Table S2 collects the different $\theta_{Au_{island}}$ values according the decomposition mechanism.

Table S2. Data resulting from different decomposition degree of a single AuNC.

Decomposition Mechanism	Reaction	n_{RS}	n_{Au}	$\theta_{Au_{island}}$
1	$Au_{13}(RS\text{-}Au\text{-}(RS)\text{-}Au\text{-}RS)_{12} \xrightarrow{Au(111)} 6(RS\text{-}Au\text{-}(RS)\text{-}Au\text{-}RS)_{Au(111)} + 13\ Au_{Au(111)}$	18	13	0.18
2	$Au_{13}(RS\text{-}Au\text{-}(RS)\text{-}Au\text{-}RS)_{12} \xrightarrow{Au(111)} 18(RS)_{Au(111)} + 25\ Au_{Au(111)}$	18	25	0.35
3	$Au_{13}(RS\text{-}Au\text{-}(RS)\text{-}Au\text{-}RS)_{12} \xrightarrow{Au(111)} 9(RS\text{-}Au\text{-}RS)_{Au(111)} + 16\ Au_{Au(111)}$	18	16	0.22

Estimation of the diffusion coefficient of mobile species

Figure S4 a-b shows that the boundary size (**d**) of the two c(4×2) domains I and II increases with time (**t**). If the domain boundaries move by incorporation of mobile species, the surface diffusion coefficient (**D**) can be estimated using the Einstein relationship:

$$\mathbf{D} = \frac{\mathbf{d}^2}{2\mathbf{t}} \qquad [S6]$$

The **d** values were obtained by analysis of the height profiles (Figures S4a-c). By using the *multiple profile* tool provided by WSxM software, the height profiles were simultaneously obtained for both images along the black and blue lines shown in images (a) and (b) respectively. The height profiles show two regions: one corresponding to the region between I and II domains and the other one to the domain II. The length of each region was determined from the four height profiles for the two consecutive images, as shown Figure S4c. Thus, **d** was determined accordingly to $\mathbf{d} = \frac{|y^i_{350} - y^i_0|}{2}$ - being i= a or b (see

figure S4c). Finally, by using the equation S6 the **D** values was obtained for each region, which gives an average **D** of $(8\pm3)\times10^{-17}$ cm^2s^{-1}.

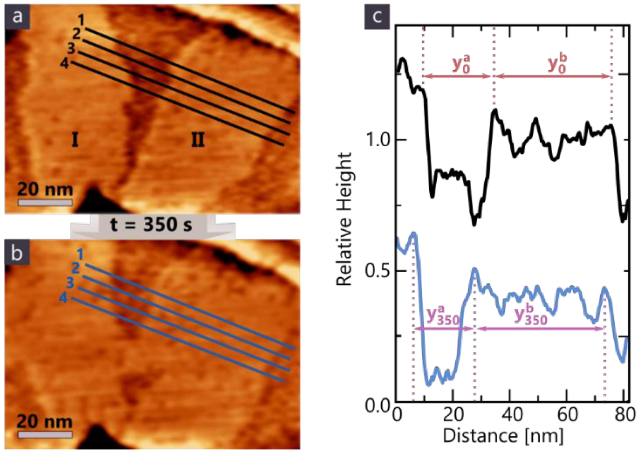

Figure S4. Estimation of the diffusion coefficient of mobile species by STM images taken in mesitylene. (a-b) Two consecutive STM images upon AuNC decomposition showing that the two c(4×2) domains (I and II) grow over a time period of 350 s. (c) Height profile along the lines 2 in images (a) and (b). The length of each region was determined by direct measuring of the distance (y_t^i , being i: a or b and t:0 or 350).

References

(1) Pensa, E.; Albrecht, T., Controlling the Dynamic Instability of Capped Metal Nanoparticles on Metallic Surfaces. *J. Phys. Chem. Lett.* **2018,** *9* (1), 57-62.

(2) Parker, J. F.; Weaver, J. E. F.; McCallum, F.; Fields-Zinna, C. A.; Murray, R. W., Synthesis of Monodisperse [Oct4N+][Au25(SR)18−] Nanoparticles, with Some Mechanistic Observations. *Langmuir* **2010,** *26* (16), 13650-13654.

(3) Horcas, I.; Fernández, R.; Gómez-Rodríguez, J. M.; Colchero, J.; Gómez-Herrero, J.; Baro, A. M., WSXM: A software for scanning probe microscopy and a tool for nanotechnology. *Rev. Sci. Instrum* **2007,** *78* (1), 013705.

(4) Angerstein-Kozlowska, H.; Conway, B. E.; Hamelin, A.; Stoicoviciu, L., Elementary steps of electrochemical oxidation of single-crystal planes of Au Part II. A chemical and structural basis of oxidation of the (111) plane. *J. Electroanal. Chem. Interf. Electrochem.* **1987,** *228* (1), 429-453.

(5) Pensa, E.; Cortés, E.; Corthey, G.; Carro, P.; Vericat, C.; Fonticelli, M. H.; Benítez, G.; Rubert, A. A.; Salvarezza, R. C., The Chemistry of the Sulfur–Gold Interface: In Search of a Unified Model. *Acc. Chem. Res.* **2012,** *45* (8), 1183-1192.

(6) Kresse, G.; Joubert, D., From ultrasoft pseudopotentials to the projector augmented-wave method. *Phys. Rev. B* **1999,** *59* (3), 1758-1775.

(7) Kresse, G.; Hafner, J., Ab initio molecular dynamics for liquid metals. *Phys. Rev. B* **1993,** *47* (1), 558-561.

(8) Kresse, G.; Furthmüller, J., Efficiency of ab-initio total energy calculations for metals and semiconductors using a plane-wave basis set. *Comput. Mater. Sci.* **1996,** *6* (1), 15-50.

(9) Kresse, G.; Furthmüller, J., Efficient iterative schemes for ab initio total-energy calculations using a plane-wave basis set. *Phys. Rev. B* **1996,** *54* (16), 11169-11186.

(10) Blöchl, P. E., Projector augmented-wave method. *Phys. Rev. B* **1994,** *50* (24), 17953-17979.

(11) Grimme, S., Semiempirical GGA-type density functional constructed with a long-range dispersion correction. *Journal of Computational Chemistry* **2006,** *27* (15), 1787-1799.

(12) Grimme, S.; Antony, J.; Ehrlich, S.; Krieg, H., A consistent and accurate ab initio parametrization of density functional dispersion correction (DFT-D) for the 94 elements H-Pu. *J. Chem. Phys.* **2010,** *132* (15), 154104.

(13) Pearson, W. B., *A Handbook of Lattice Spacings and Structures of Metals and Alloys*. Pergamon Press: 1958.

(14) Monkhorst, H. J.; Pack, J. D., Special points for Brillouin-zone integrations. *Phys. Rev. B* **1976,** *13* (12), 5188-5192.